# Interface Modulation Boosts Nitrate Reduction Performance of Iron-based Catalysts

Jianlong Ma[†a], Jiahao An[†a], Yunpeng Zuo[b], Huimin Jia[a], Wenbiao Zhang*[c] and Tingting Li*[a]

[a]Key Laboratory of Micro-Nano Materials for Energy Storage and Conversion of Henan Province, Institute of Surface Micro and Nano Materials, College of Chemical and Materials Engineering, Xuchang University, Xuchang, Henan, 461000 P. R. China.
E-mail: tingtingli101@xcu.edu.cn

[b]Key Laboratory of Materials Physics, Ministry of Education, School of Physics, Zhengzhou University, Zhengzhou, China.

[c]College of Chemistry and Materials Science, Jinan University,Guangzhou 510632, P.R. China.
E-mail: wbzhang@jnu.edu.cn

# SUPPORTING INFORMATION

## 1. Experimental Section

**Chemical Reagents:** All chemicals were used as received without further purification. Deionized water was used throughout the experimental process. Sodium nitrate ($NaNO_3$, AR, 99%), sodium potassium tartrate tetrahydrate ($KNaC_4H_4O_6 \cdot 4H_2O$, AR, 99%), sodium salicylate ($C_7H_5O_3Na$, AR, 99%), ammonium chloride ($NH_4Cl$, AR, 98%), and iron(III) oxide ($Fe_2O_3$, AR) were purchased from Sinopharm Chemical Reagent Co., Ltd. Potassium hydroxide (KOH, AR, >85%) and sodium hypochlorite solution (NaClO, available chlorine ≥5.0%) were obtained from Shanghai Aladdin Biochemical Technology Co., Ltd. Sodium nitroprusside ($C_5H_4FeN_6Na_2O_3$, AR, >99%) and Nafion 117 solution (5%) were supplied by Shanghai Macklin Biochemical Technology Co., Ltd.

**Materials Characterization:** The microscopic morphology of the materials was characterized using a FEI Titan HRTEM transmission electron microscope operated at 300 kV for high-resolution imaging and elemental mapping. Surface elemental composition and chemical states were analyzed by X-ray photoelectron spectroscopy (XPS) on a Thermo Scientific Escalab 250Xi spectrometer with an Al Kα X-ray source (1486.6 eV). Powder X-ray diffraction (XRD) patterns were collected using a Bruker D8 ADVANCE diffractometer (Germany). Inductively coupled plasma mass spectrometry (ICP-MS) was tested using an Agilent-7900 system. Ultraviolet-visible (UV-Vis) spectra were recorded on an Agilent Cary 5000 spectrophotometer (USA). Raman spectra were acquired using a HORIBA LabRAM HR Evolution Raman spectrometer (Japan). Fourier-transform infrared (FTIR) absorption spectra were measured with a Bruker VERTEX 80v spectrometer (Germany) equipped with a mercury-cadmium-telluride (MCT) cryogenic detector. X-ray absorption fine structure (XAFS) spectra at the Fe K-edge were collected at the BL14W1 beamline of the Shanghai Synchrotron Radiation Facility (SSRF). The raw XAFS data were processed using the ATHENA module in the IFEFFIT software package, and fitting was

performed with the ARTEMIS module utilizing a Hanning window with a width of 1.0 $Å^{-1}$. Electrochemical measurements were carried out using a CHI660E electrochemical workstation (Shanghai Chenhua).

**Material Synthesis:** A specified mass of sodium nitroprusside ($C_5FeN_6Na_2O·2H_2O$) was weighed and placed in a clean porcelain boat, which was then positioned in a tube furnace. Under an argon atmosphere, the temperature was raised to 900 °C at a heating rate of 10 °C $min^{-1}$, maintained for 2 hours for pyrolysis, and then allowed to cool freely to room temperature. The resulting product was collected and ground into fine particles to obtain the final Fe@CN material.

**Electrode Preparation:** 6 mg of Fe@CN powder was weighed and dissolved in 100 μL of a 10-fold diluted Nafion 117 perfluorinated resin solution. The mixture was ultrasonicated for 20 minutes until a homogeneous ink-like dispersion was formed. A carbon paper was clamped with an electrode clip, exposing an area greater than 1 $cm^2$. Then, 30 μL of the homogeneous ink was drop-cast onto the carbon paper, covering a fixed area of 1 $cm^2$. After drying, an additional 20 μL of Nafion solution was coated on the surface to form a protective layer. The as-prepared electrode was used as the working electrode.

**Electrochemical Measurements:** The electrochemical performance of the catalyst was evaluated using a CHI660E electrochemical workstation. A standard three-electrode system was employed, consisting of a platinum sheet as the counter electrode, an Hg/HgO electrode as the reference electrode, and the carbon paper coated with the Fe@CN catalyst as the working electrode. All tests were conducted in an H-type electrolytic cell. The cathode chamber was filled with an aqueous solution of 1 M KOH and 0.5 M $NaNO_3$, while the anode chamber contained a 1 M KOH solution. The two chambers were separated by a Nafion 117 proton exchange membrane to prevent the re-oxidation of cathodic reduction products at the anode.

The electrochemical performance was evaluated using two primary methods: linear sweep voltammetry (LSV) and chronoamperometry (i-t). Initially, LSV was employed for a preliminary assessment of the electrocatalytic activity. Prior to each LSV measurement, one cycle of cyclic voltammetry (CV) was performed to activate

the catalyst and stabilize the electrochemical interface. The LSV scans were conducted from 0.2 to -0.7 V vs. RHE at a scan rate of 2 mV $s^{-1}$. Based on the LSV results, five distinct potentials were selected for i-t measurements, each with a duration of 1000 s. The electrolyte was replaced before each test to eliminate any residual effects from previous measurements. Following each i-t test, the electrolyte from the cathode chamber was collected, sealed in a 10 mL centrifuge tube, and stored for subsequent quantitative analysis of the $NH_3$ product via UV-Vis spectroscopy to determine the *e*-$NO_3$RR performance.

**Quantification of the $NH_3$ Product:** The concentration of $NH_3$ produced via electrocatalytic nitrate reduction was determined by the indophenol blue method using a UV-Vis spectrophotometer. Three color-developing reagents were prepared in advance:

Reagent A: 5 g of sodium salicylate and 5 g of sodium potassium tartrate tetrahydrate were dissolved in 100 mL of a 1 M KOH aqueous solution.

Reagent B: 0.05 M sodium hypochlorite (NaClO) solution, stored in the dark.

Reagent C: 0.01 g $mL^{-1}$ sodium nitroprusside solution.

Standard Solution Preparation and Calibration: A small amount of ammonium chloride ($NH_4Cl$) was dissolved in a 1 M KOH solution to prepare a stock solution, which was then sequentially diluted to create a concentration gradient ranging from 0.01 to 0.08 mmol $L^{-1}$. Aliquots of these standard solutions with varying concentrations were pipetted into 7 mL centrifuge tubes. Each aliquot was then supplemented with 1 M KOH to a total volume of 2 mL. Subsequently, 2 mL of Reagent A, 1 mL of Reagent B, and 0.2 mL of Reagent C were added sequentially and mixed thoroughly. The resulting mixtures were incubated in the dark for 2 hours to allow for complete color development. The UV-Vis spectra of the solutions were then recorded in the wavelength range of 620–680 nm. The absorbance peak at approximately 655 nm was measured, and a standard calibration curve was established by plotting the peak absorbance against the corresponding known $NH_3$ concentrations.

Quantification of $NH_3$ in Post-Test Electrolyte: The electrolyte collected after each i-t test was appropriately diluted based on the passed charge. Aliquots of the diluted

samples were pipetted into 7 mL centrifuge tubes, followed by the addition of deionized water to bring the total volume to 2 mL. Subsequently, 2 mL of Reagent A, 1 mL of Reagent B, and 0.2 mL of Reagent C were added sequentially and mixed thoroughly. The resulting solution was kept in the dark for 2 hours to allow for complete color development. The UV-Vis measurement was performed following the same procedure described above. The obtained maximum absorbance value was then interpolated from the standard calibration curve to calculate the concentration of the produced $NH_3$.

The FE for electrocatalytic nitrate reduction to $NH_3$ was calculated using the following equation:

$$\mathrm{FE} = \frac{8F \times C_{\mathrm{NH_3}} \times V}{Q}$$

The $NH_3$ yield rate was calculated as:

$$\mathrm{Yield}_{\mathrm{NH_3}} = \frac{C_{\mathrm{NH_3}} \times V}{t \times S}$$

Where $F$ is the Faraday constant (96485 C $mol^{-1}$), $C_{NH3}$is the molar concentration of produced $NH_3$ (mol $L^{-1}$), $V$ is the volume of the electrolyte in the cathode chamber (L), $Q$ is the total charge passed during electrolysis (C), $t$ is the electrolysis time (h), and $S$ is the geometric area of the working electrode ($cm^2$).

**2. Supporting Figures**

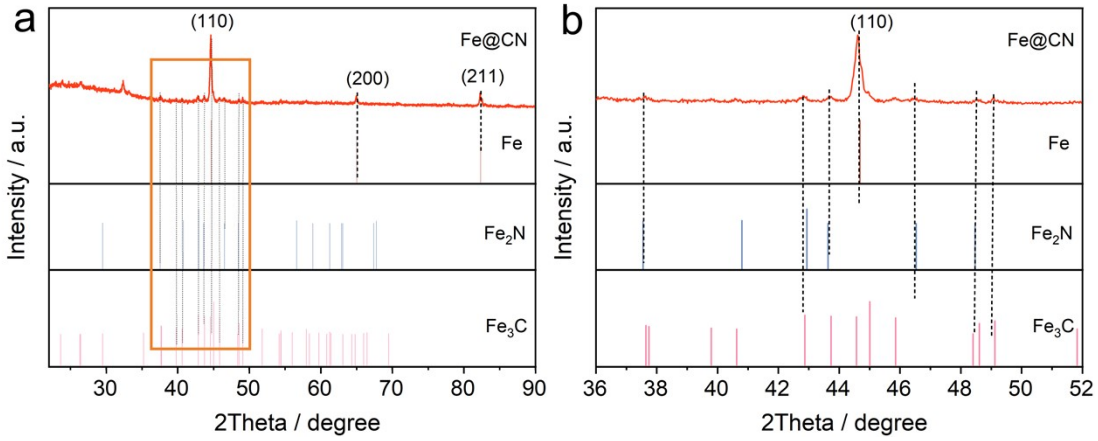


**Fig. S1** (a) XRD patterns of the Fe@CN sample and the reference Fe, $Fe_2N$ and $Fe_3C$, (b) The enlarged view of the area within the box in (a).

**Table S1.** ICP measurement for Fe content in Fe@CN.

| **Element** | **Weight(g)** | **Volume(mL)** | **Dilution factor** | **Gauge reading (mg $L^{-1}$)** | **Mass fraction** |
|---|---|---|---|---|---|
| Fe | 0.0219 | 50 | 50 | 7.3591 | 84.01% |

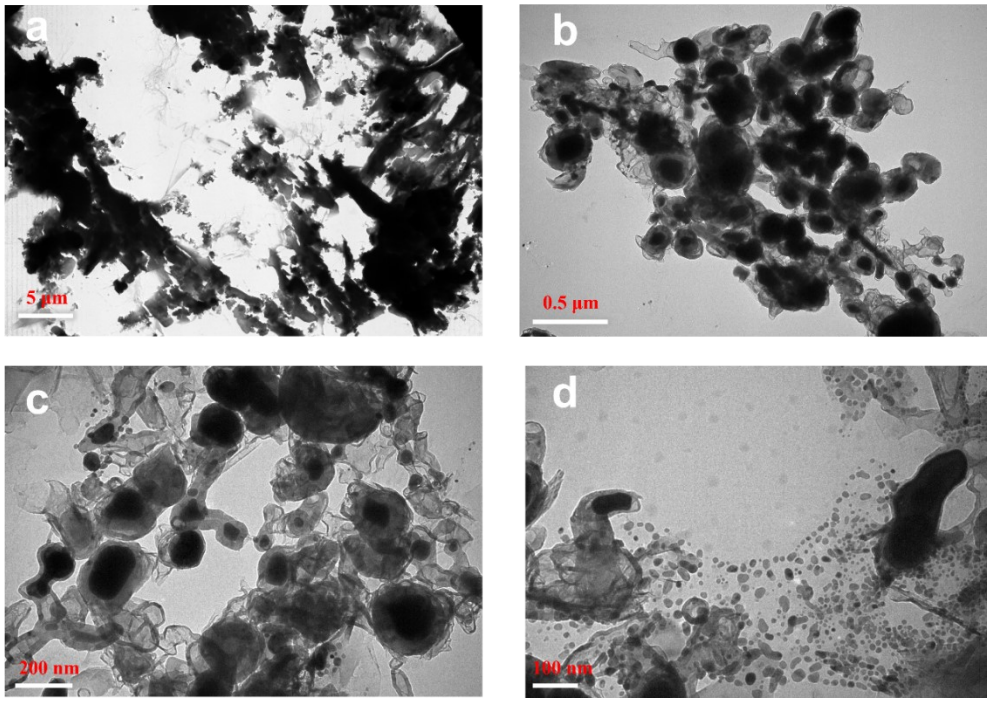


**Fig. S2** TEM images of Fe@CN at different magnifications.

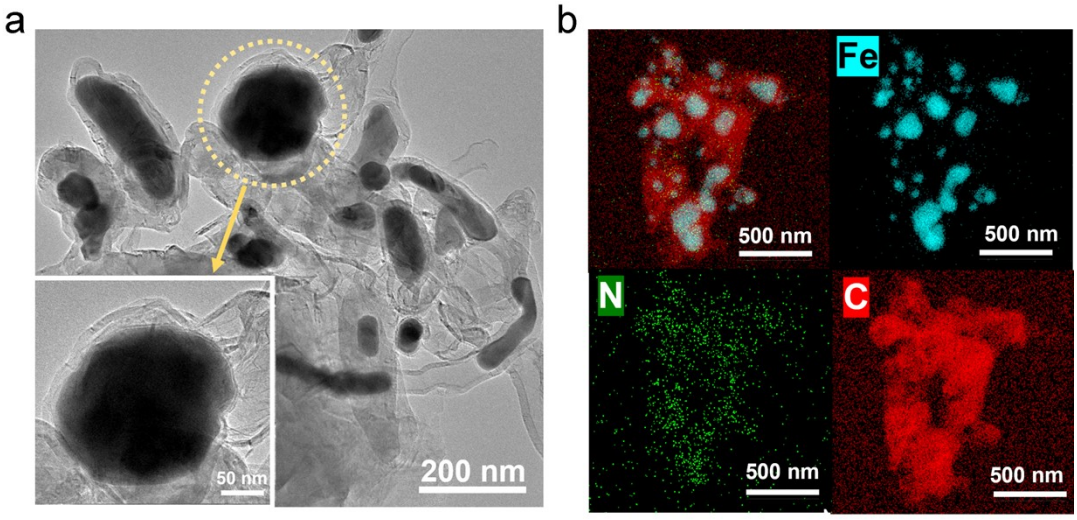


**Fig. S3** (a) TEM and (b) EDS mapping images of the Fe@CN.

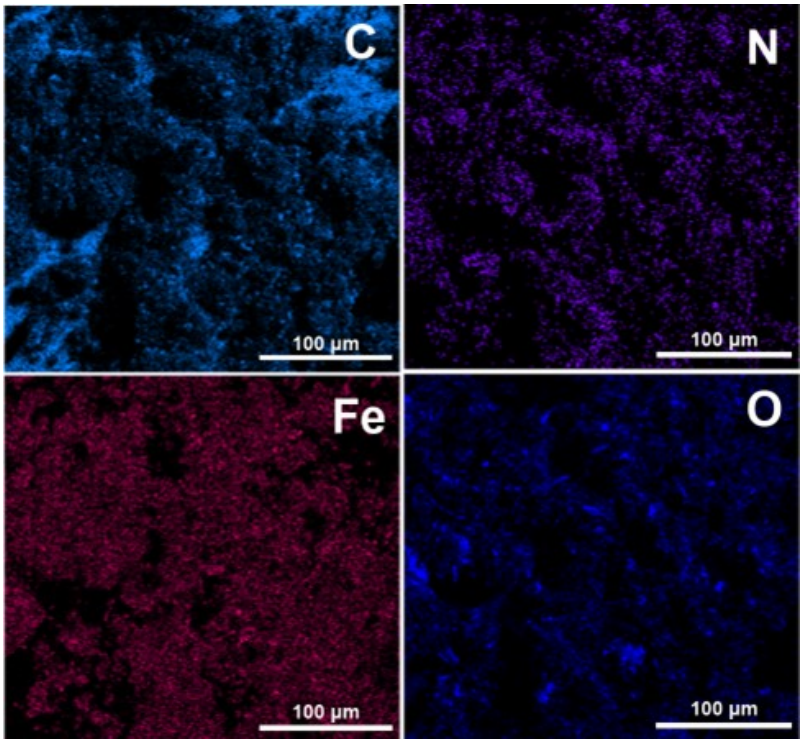


**Fig. S4** SEM-EDS mapping of C, N, Fe and O element.

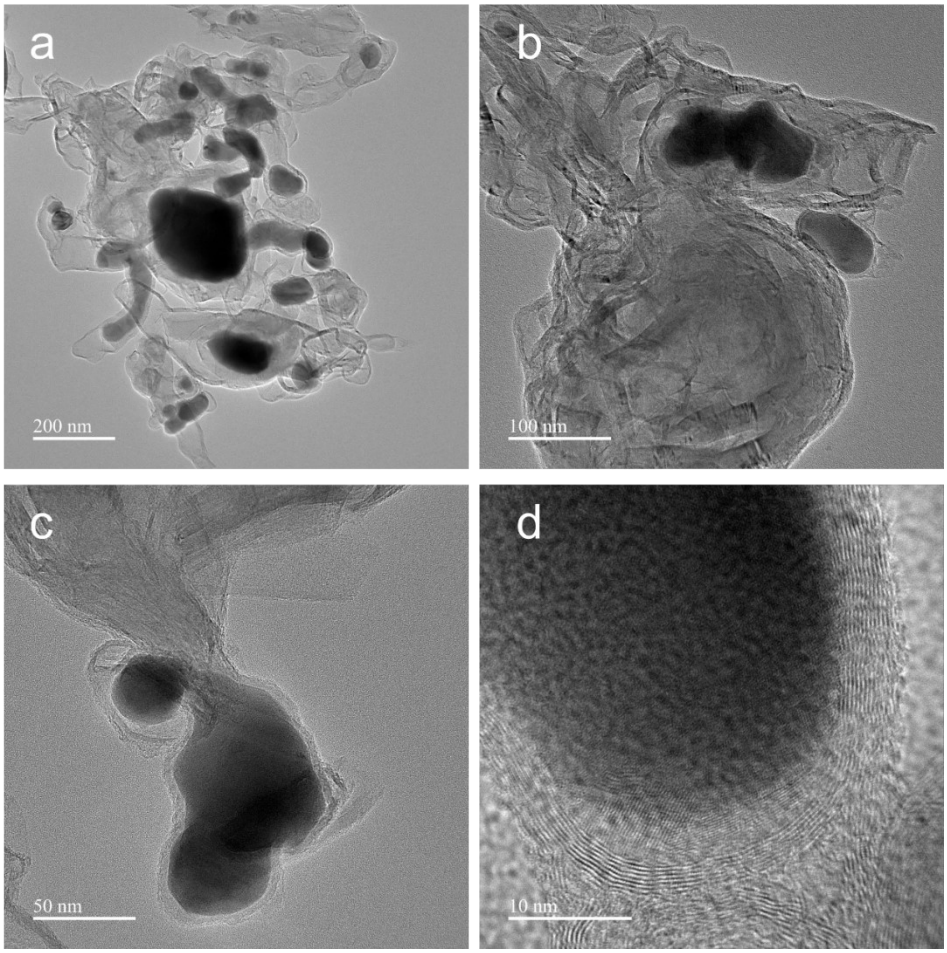


**Fig. S5** HRTEM images of Fe@CN at different magnifications.

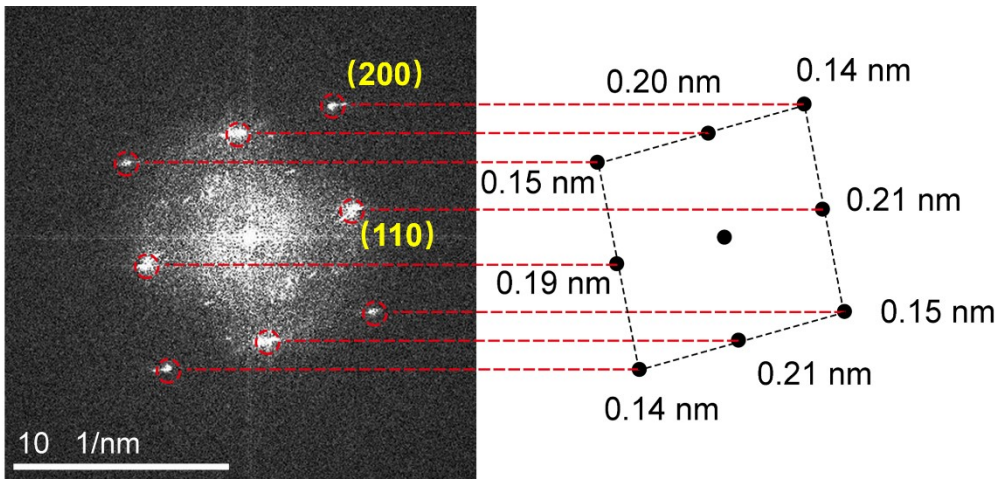


**Fig. S6** SAED pattern of Fe@CN.

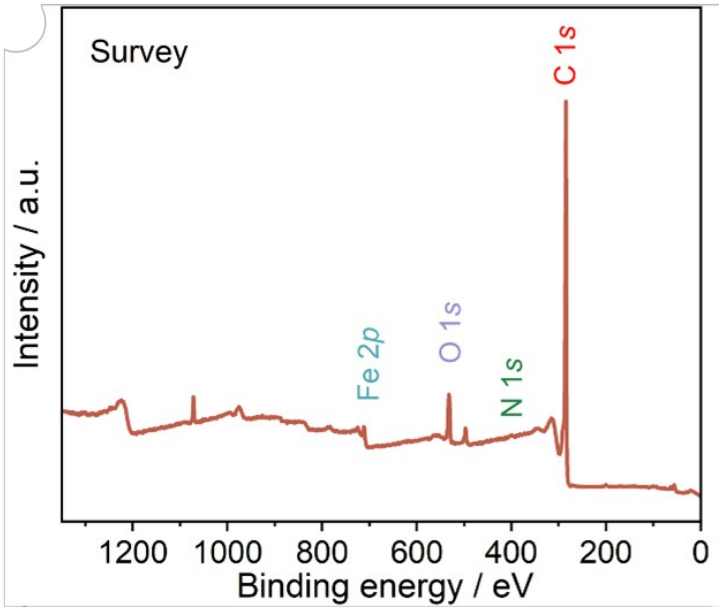


**Fig. S7** XPS spectra of Fe@CN.

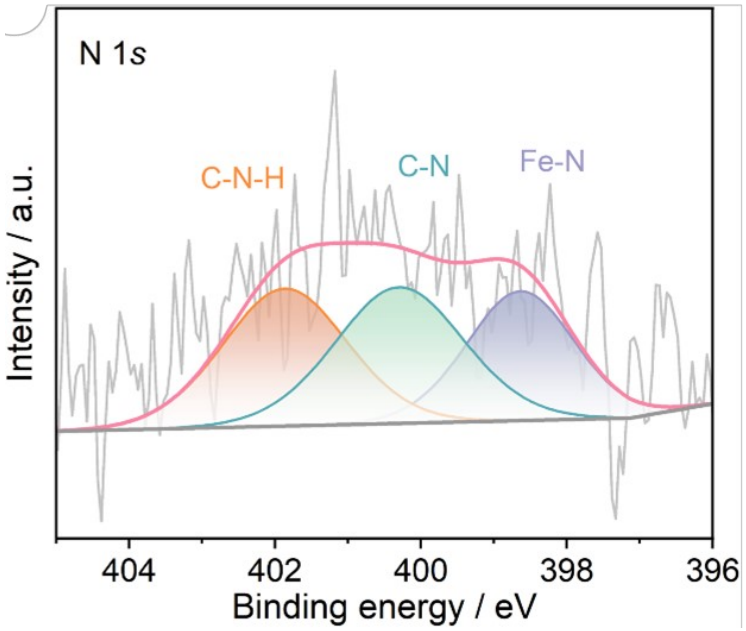


**Fig. S8** N 1s spectra of Fe@CN.

**Table S2.** The elemental composition (C and N) in the Fe@CN catalyst measured by organic elemental analysis.

| **Element** | C | N | H | S |
|---|---|---|---|---|
| **Percentage (%)** | 27.69 | 4.42 | 0.175 | 0.022 |

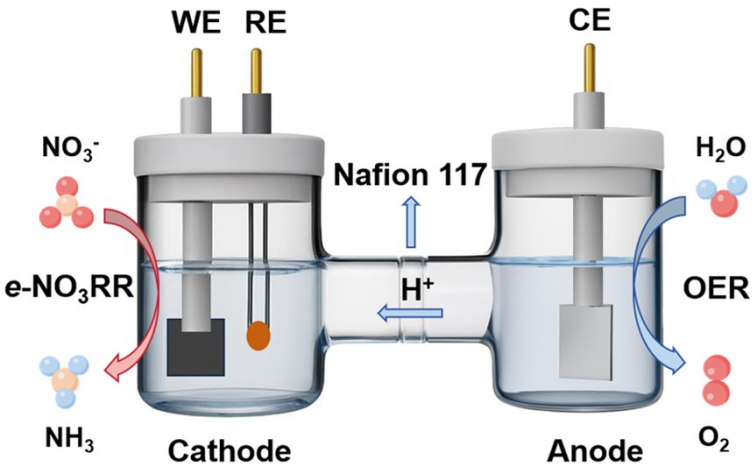


**Fig. S9** Schematic diagram of the H-type electrolytic cell.

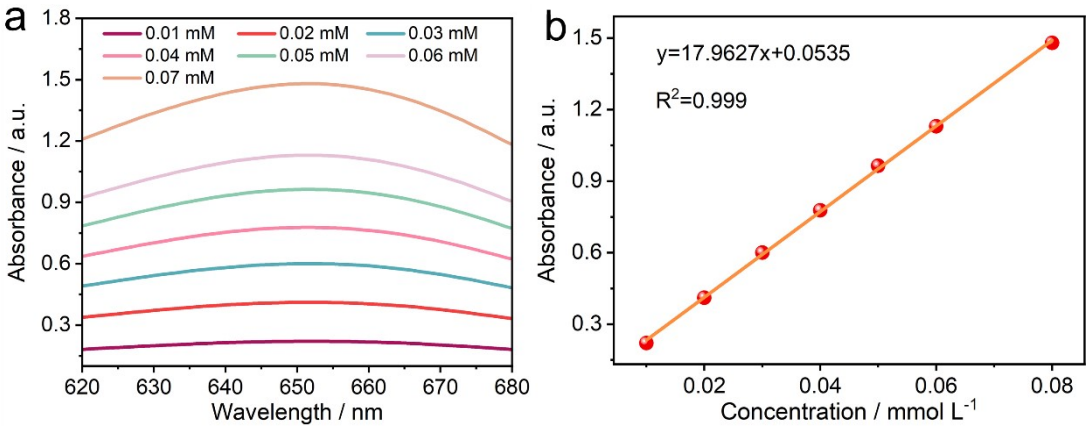


**Fig. S10** (a) UV-Vis spectra of $NH_4Cl$ solutions at varying concentrations; (b) Standard curve for ammonia after linear fitting.

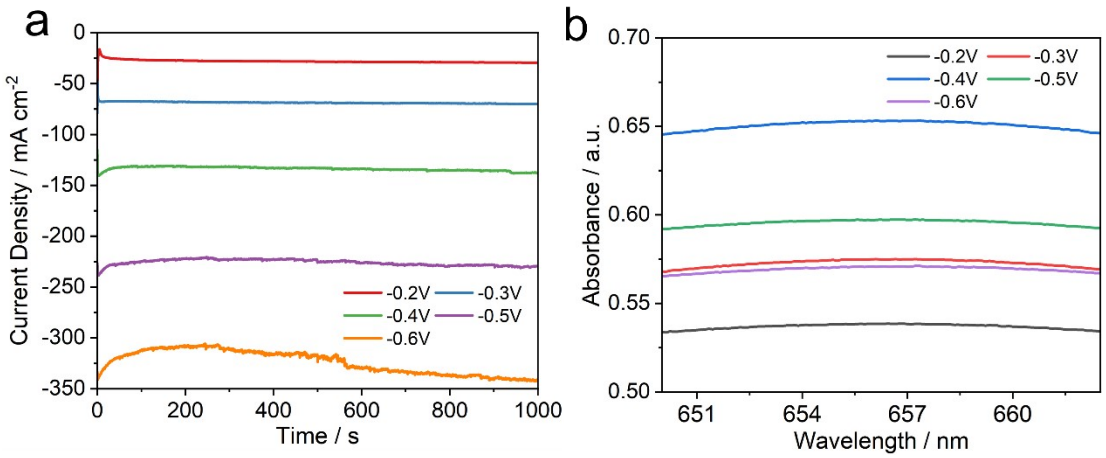


**Fig. S11.** (a) i-t curves at different applied voltages; (b) UV-Vis spectra of the electrolytes after electrolysis at different voltages.

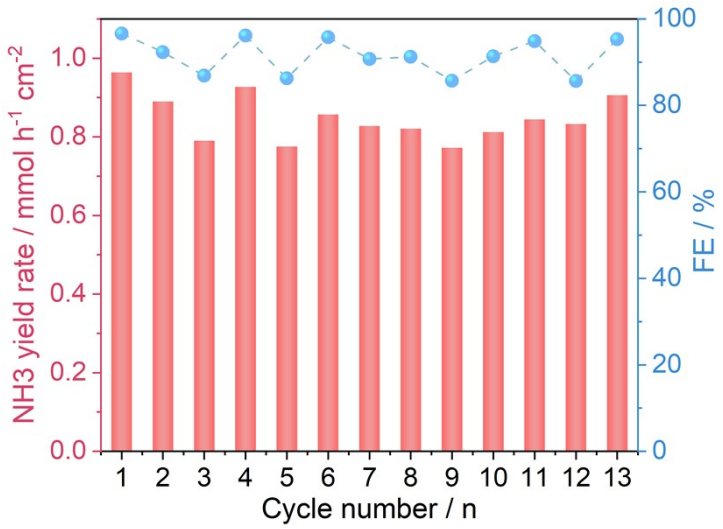


**Fig. S12** $NH_3$ yield rate and corresponding FE measured at regular intervals during the stability test for Fe@CN.

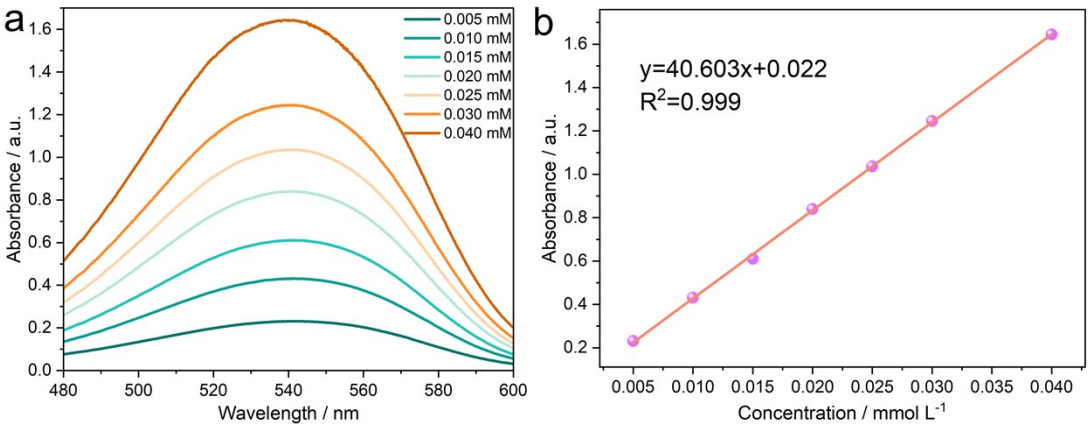


**Fig. S13** (a) UV-Vis spectra of $NO_2^-$ solutions with different concentrations; (b) Calibration curve for $NO_2^-$ after linear fitting.

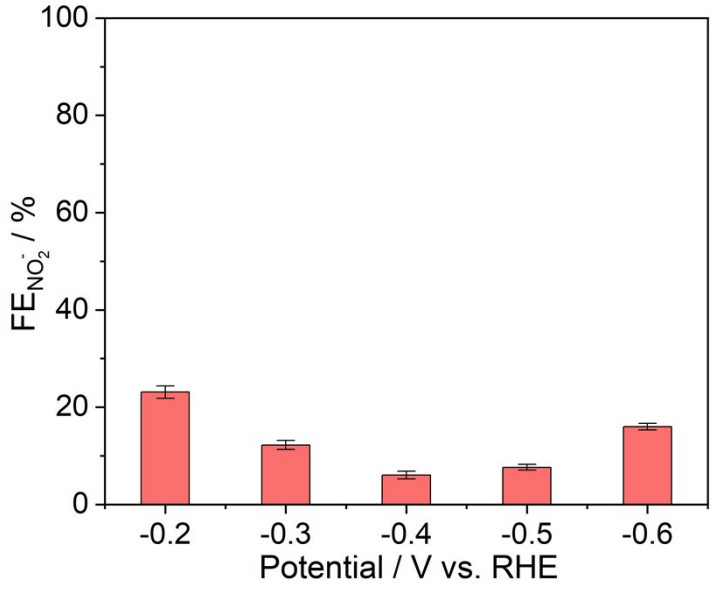


**Fig. S14** Faradaic efficiency of $NO_2^-$ measured on Fe@CN at various applied potentials.

**Table S3.** Comparison of $NO_3^-$RR performance of Fe@CN with the reported catalysts at −0.4 V vs. RHE.

| No. | Catalyst | FE (%) | $NH_3$ Yield Rate (mmol $h^{-1}$ $cm^{-2}$) | Current Density (mA $cm^{-2}$) | Reference |
|---|---|---|---|---|---|
| **1** | **Fe@CN** | **97.2** | **0.603** | **104.3** | **This work** |
| 2 | $Fe_3C$/NC | 96.7 | 0.269 | 65.6 | SI Ref.[1] |
| 3 | $FeS_2$@$TiO_2$ | 97 | 0.320 | 70.7 | SI Ref.[2] |
| 4 | Fe-$Co_3O_4$/PC | 90 | 0.400 | 95.3 | SI Ref.[3] |
| 5 | Fe-BCN | 80 | 0.265 | 70.9 | SI Ref.[4] |
| 6 | FeP@$TiO_2$/TP | 92 | 0.250 | 58.3 | SI Ref.[5] |
| 7 | Fe/$Ni_2P$ | 94.3 | 0.245 | 55.8 | SI Ref.[6] |
| 8 | Fe/Cu-HNG | 84 | 0.110 | 28.2 | SI Ref.[7] |
| 9 | RuFe NFs | 80 | 0.103 | 27.6 | SI Ref.[8] |
| 10 | Cu-Pd/C nanobelts | 62.3 | 0.013 | 4.5 | SI Ref.[9] |
| 11 | $Bi_1Pd$ | 90 | 0.441 | 105 | SI Ref.[10] |
| 12 | Pd-PdO/rGO | 52 | 0.174 | 71.7 | SI Ref.[11] |
| 13 | PdCu/$Cu_2O$ | 68 | 0.101 | 32 | SI Ref.[12] |
| 14 | Pd/$TiO_2$ | 40 | 0.002 | 40 | SI Ref.[13] |

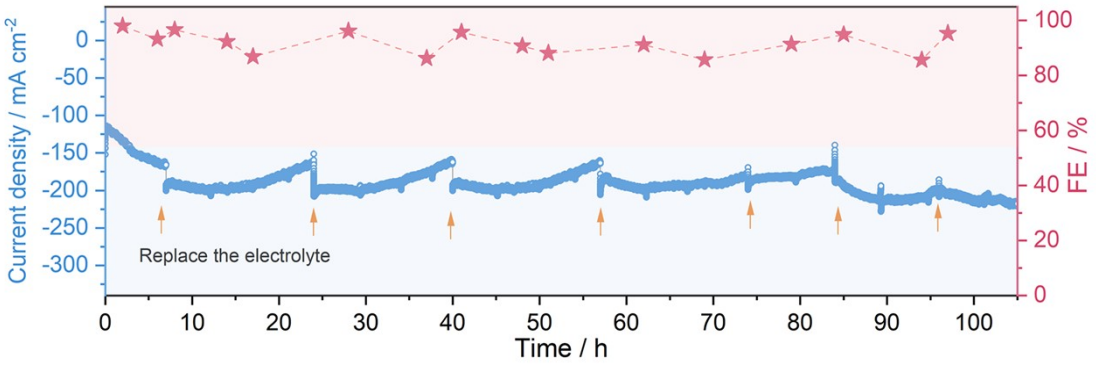


**Fig. S15** Long-term i-t test of Fe@CN at -0.4 V vs. RHE over 105 hours and its associated FE for $NH_3$ production.

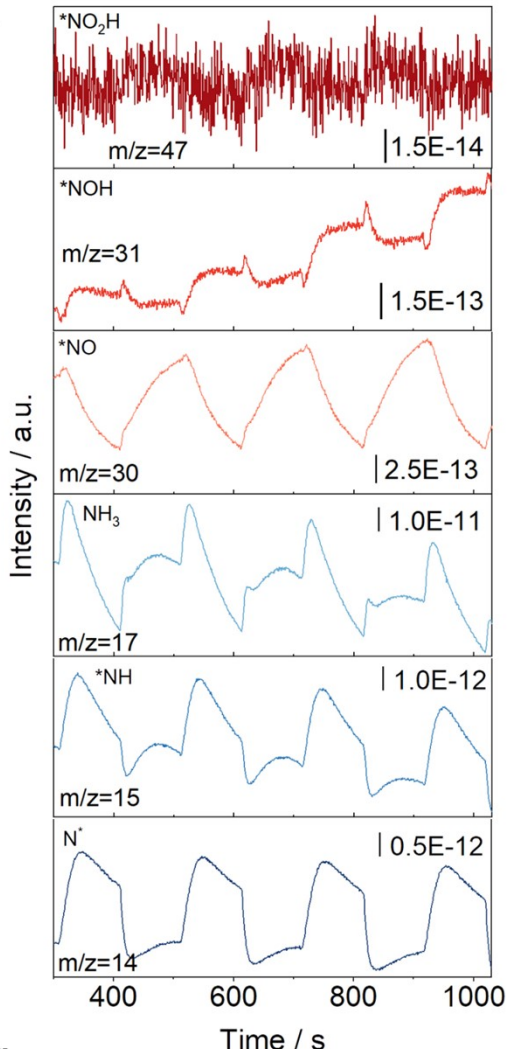


**Fig. S16** Online DEMS measurements of Fe@CN during electrocatalytic nitrate reduction.

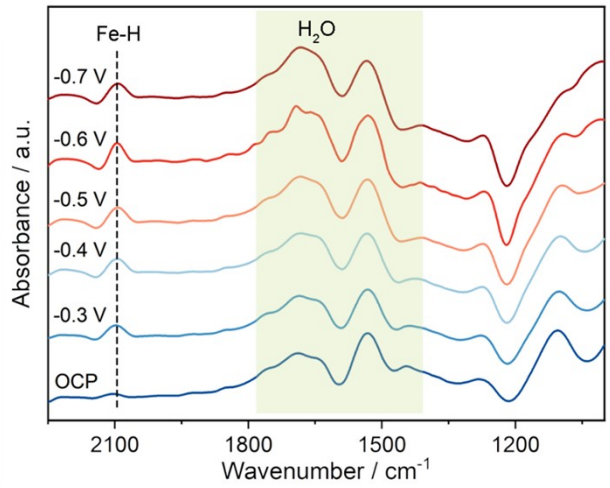


**Fig. S17** *In situ* ATR-SEIRAS spectra of Fe@CN measured in KOH without $NO_3^-$ under various applied potentials.

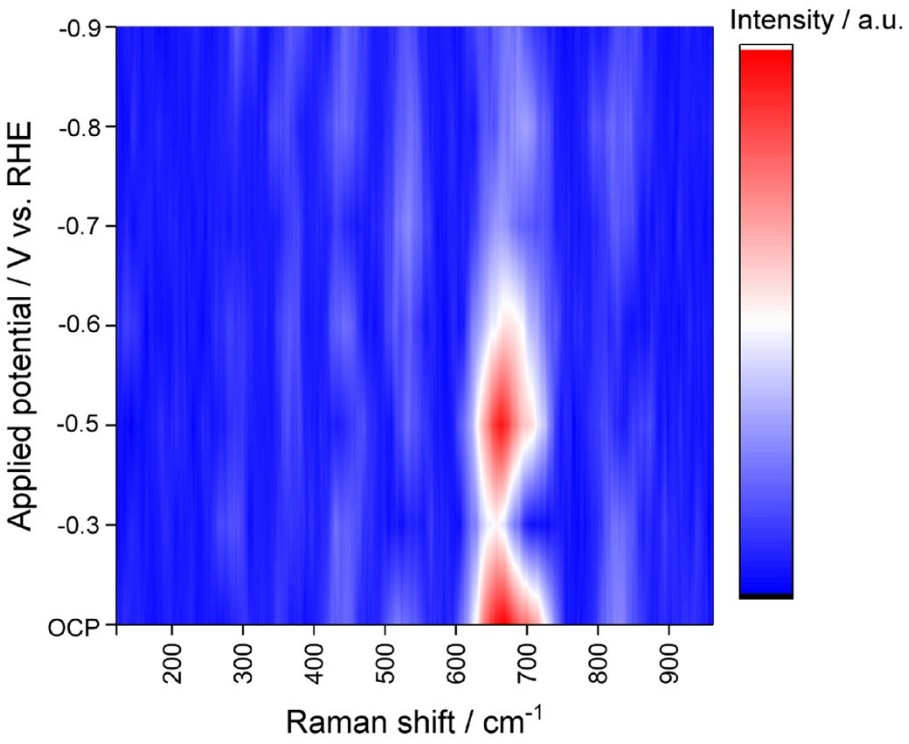


**Fig. S18** *In situ* Raman spectra of Fe@CN acquired at different applied potentials.

## References


[1] Y. Wang, L. Zhang, Y. Niu, D. Fang, J. Wang, Q. Su, C. Wang, *Green Chem*. **2021**, *23*, 7594.

[2] H. Wang, D. Zhao, C. Liu, X. Fan, Z. Li, Y. Luo, D. Zheng, S. Sun, J. Chen, J. Zhang, Y. Liu, S. Gao, F. Gong, X. Sun, *J. Mater. Chem. A*, **2022**, *10*, 24462.

[3] X. Liu, C. Liu, X. He, Z. Cai, K. Dong, J. Li, X. Fan, T. Xie, X. Yang, Y. Luo, D. Zheng, S. Sun, S. Alfaifi, F. Gong, X. Sun, *Nano Res*. **2024**, *17*, 2276.

[4] X. Lu, J. Wei, H. Lin, Y. Li, Y.-Y. Li, *ACS Appl. Nano Mater*. **2024**, *7*, 14654.

[5] A. Zhang, Y. Liang, X. He, X. Fan, C. Yang, L. Ouyang, D. Zheng, S. Sun, Z. Cai, Y. Luo, Q. Liu, S. Alfaifi, L. Cai, H. Wang, X. Sun, *Inorg. Chem*. **2023**, 62, 12644.

[6] R. Zhang, Y. Guo, S. Zhang, D. Chen, Y. Zhao, Z. Huang, L. Ma, P. Li, Q. Yang, G. Liang, C. Zhi, *Adv. Energy Mater*. **2022**, 12, 2103872.

[7] S. Zhang, J. Wu, M. Zheng, X. Jin, Z. Shen, Z. Li, Y. Wang, Q. Wang, X. Wang, H. Wei, J. Zhang, P. Wang, S. Zhang, L. Yu, L. Dong, Q. Zhu, H. Zhang, J. Lu, *Nat. Commun*. **2023**, 14, 3634.

[8] Y. Wang, M. Sun, J. Zhou, Y. Xiong, Q. Zhang, C. Ye, X. Wang, P. Lu, T. Feng, F. Hao, F. Liu, J. Wang, Y. Ma, J. Yin, S. Chu, L. Gu, B. Huang, Z. Fan, *PNAS*, **2023**, 120, e2306461120.

[9] Z. Wang, C. Sun, X. Bai, Z. Wang, X. Yu, X. Tong, Z. Wang, H. Zhang, H. Pang,L. Zhou, W. Wu, Y. Liang, A. Khosla, Z. Zhao, *ACS Appl. Mater. Interfaces*, **2022**, 14, 30969.

[10] K. Chen, Z. Ma, X. Li, J. Kang, D. Ma, K. Chu, *Adv. Funct. Mater.*, **2023**, 33, 2209890.

[11] J. Ebenezer, A. Lal, P. Velayudham, A. Borenstein, A. Schechter, *ACS Appl. Mater. Interfaces*, **2024**, 16, 36433.

[12] H. Yin, Z. Chen, S. Xiong, J. Chen, C. Wang, R. Wang, Y. Kuwahara, J. Luo, H. Yamashita, Y. Peng, J. Li, *Chem Catalysis*, **2021**, 1, 1088.

[13] Y. Guo, R. Zhang, S. Zhang, Y. Zhao, Q. Yang, Z. Huang, B. Dongb, C. Zhi, *Energy Environ. Sci.*, **2021**, 14, 3938.